Am J Transl Res 2019;11(9):6007-6015
www.ajtr.org /ISSN:1943-8141/AJTR0100014

Original Article

ImmunoPET imaging of CD38 expression in hepatocellular carcinoma using ^{64}Cu-labeled daratumumab

Shiyong Li[1,2], Christopher G England[2], Emily B Ehlerding[2], Christopher J Kutyreff[2], Jonathan W Engle[2], Dawei Jiang[2], Weibo Cai[2]

[1]*Department of Rehabilitation, Second Affiliated Hospital of Nanchang University, Nanchang 330006, Jiangxi, China;* [2]*Department of Radiology and Medical Physics, University of Wisconsin-Madison, WI 53705, United States*

Received July 18, 2019; Accepted August 6, 2019; Epub September 15, 2019; Published September 30, 2019

Abstract: CD38 is expressed on the surface of many immune cells, which are closely associated with antitumor immunity and immune tolerance of tumor cells. Therefore, monitoring CD38 expression has gained great attention for tracking the progression of tumors and cancer treatment. Herein, we aim to develop a PET tracer using an anti-CD38 monoclonal antibody (daratumumab) to monitor CD38 expression in hepatocellular carcinoma (HCC). In this study, daratumumab was radiolabeled with ^{64}Cu ($t_{1/2}$=12.7 h) to obtain ^{64}Cu-NOTA-daratumumab. Relative CD38 expression in HepG2 and Huh7 HCC cell lines was assessed using western blot. The specificity of ^{64}Cu-NOTA-daratumumab to both cell lines was examined using an in vitro cell-binding assay. PET imaging in subcutaneous models of HCC was performed to evaluate the capability and specificity of ^{64}Cu-NOTA-daratumumab to target CD38 in vivo. Region-of-interest analysis and ex vivo biodistribution were performed to verify the tracer targeting capability of CD38. Through cellular studies of two HCC cell lines, CD38 expression was found to be higher in HepG2 and minimal in Huh7 cells. ^{64}Cu-NOTA-daratumumab showed relatively high affinity to CD38 (K_a=18.21 ± 1.74 nM), while the affinity of Huh7 was in the micromolar range for daratumumab binding to the cells (K_a=3.98 ± 0.87 μM). At 48 h post-injection, PET imaging of subcutaneous models with ^{64}Cu-NOTA-daratumumab revealed tumor uptakes of 12.23 ± 2.4 and 2.7 ± 1.2 %ID/g for HepG2 and Huh7, respectively (n=4), which correlated well with relative CD38 expression of the cells. Moreover, the ^{64}Cu-NOTA-IgG nonspecific analogue showed a significantly lower uptake in HepG2 subcutaneous model in mice, suggesting a specific binding of daratumumab with CD38 in vivo. Our cellular studies and PET imaging confirmed the capability and specificity of ^{64}Cu-NOTA-daratumumab for the imaging of CD38 in murine models of HCC. This study supports our claim that ^{64}Cu-NOTA-daratumumab is an effective PET tracer for the non-invasive evaluation of CD38 expression and sensitive detection of CD38-positive tumor lesions in HCC.

Keywords: Positron emission tomography, daratumumab, CD38, hepatocellular carcinoma, molecular imaging

Introduction

Hepatocellular carcinoma (HCC) is a leading cause of cancer-related death worldwide [1]. Despite making a rapid progress in new technologies for diagnosis and treatment, incidence and mortality still maintain growth [2]. There are many risk factors for the development of HCC, such as hepatitis B, hepatitis C and alcohol abuse [3]. For example, there is the significant correlation between hepatocarcinogenicity and chronic Hepatitis B virus infection [4], and 80% of patients with hepatitis C will progress to chronic hepatitis [5]. In addition, studies in Europe demonstrated that alcohol abuse accounts for 40%-50% of all HCC cases in Europe [6]. Although patients with HCC can get significant benefits from surgery remediation, such as orthotopic liver transplantation (OLT), this specific therapy cannot be widely performed due to the shortage of available organs [7, 8]. Therefore, finding effective therapeutic strategies is still a major challenge for the treatment of HCC.

Recent understanding of various types of molecular aberrations underlying HCC's pathogenesis has revealed a variety of molecular

subclasses and gene signatures, demonstrating that molecular subclasses are correlated with HCC's clinical features [9, 10]. This will contribute to the generation of patient-tailored therapies. Yet so far, effective targeting and treatment of HCC is still limited to a group of patients who display certain molecular alterations. Therefore, it is key to find new relevant molecular markers that allow for effective targeted therapy of HCC. Molecular sub-classification of HCC tumors has been instrumental in identifying new biomarkers of drug response that might allow the emergence of novel diagnostics and therapeutic paradigms.

CD38 belongs to the ribosyl cyclase family, and is expressed on many kinds of cellular surfaces, such as that of immune cells and non-hematopoietic cells [11]. Its function has been explored in multiple immune cell types, and varies during lymphocyte development, activation, and differentiation [12]. For example, CD38 plays many important roles in regulating immune cell adhesion and signal transduction pathways [13, 14], and a high percentage of CD38-expressing leukemic cells is closely related to unfavorable prognosis of leukemia [15, 16]. Although extensive data exists describing CD38 in a variety of immune cells, noninvasive in vivo molecular imaging of CD38 in HCC tumors has remained unexplored. In this study, we devote our efforts to validate CD38 as a biomarker for noninvasive diagnosis of CD38-expressing HCC. We believe that the findings provide evidence for the clinical translation of this molecular targeting strategy.

Methods and materials

Radiolabeling of daratumumab

Radiolabeling of daratumumab with ^{64}Cu was performed through conjugation of the chelator p-SCN-Bn-NOTA (NOTA; Macrocyclics, Dallas, TX, USA) to the antibody, as described in previous protocols [17-19]. Briefly, daratumumab in 1 x PBS solution was adjusted to pH 8-8.5 using 0.1 M Na_2CO_3. NOTA was mixed with the antibody solution at a molar ratio of 1:10 (daratumumab: NOTA). After reacting for 2-3 h at room temperature, NOTA-daratumumab was purified from unconjugated NOTA by using one PD-10 column (GE Healthcare, Aurora, OH, USA). ^{64}Cu was produced in a CTI RDS 112 cyclotron via ^{64}Ni(p, n)^{64}Cu reaction and separated from the enriched nickel target. After NOTA-daratumumab was mixed with $^{64}CuCl_2$ in a 0.1 M sodium acetate buffer (pH 5.5) for 30 min at 37°C, ^{64}Cu-NOTA-daratumumab was purified, collected, and filtered before injection into mice. Similarly, the same procedure was used for radiolabeling IgG (Thermo Fisher Scientific, Waltham, MA, USA) to obtain ^{64}CuNOTA-IgG [20, 21].

Cell culture

Two HCC cell lines, HepG2 and Huh7, were obtained from the American Type Culture Collection (ATCC, Manassas, VA, USA). HepG2 cells were cultured in Dulbecco's minimum essential medium (DMEM), containing 4.5 g/L glucose, and supplemented with 10% fetal bovine serum (GibcoBRL, Grand Island, NY, USA), 1% penicillin/streptomycin, and 1% non-essential amino acids. Huh7 cells were cultured in DMEM containing 10% fetal bovine serum. All cells were maintained at 37°C in a humidified 5% CO_2 atmosphere.

Flow cytometry

Flow cytometry was used to examine the binding and immune-reactivity of daratumumab to HepG2 and Huh7 cells. After being harvested, counted, and re-suspended in PBS (1×10^6 cells/mL), cells were incubated for 30 min on ice with either PBS, 5 μg/mL of daratumumab, 25 μg/mL of daratumumab, 5 μg/mL of NOTA-daratumumab, or 25 μg/mL of NOTA-daratumumab. At the end of incubation, cells were washed with PBS buffer and then incubated with 5 μg/mL of Cy3-labeled secondary antibody for 30 min on ice. Lastly, a BD FACSAria cell sorter was used for testing samples, and data was analyzed using the FlowJo V10 software.

Saturation binding assay

^{64}Cu-NOTA-daratumumab was used to determine the cellular binding affinity in HepG2 and Huh7 cells. After being seeded in a 96-well plate (5×10^5/well), cells were incubated with increasing concentrations of ^{64}Cu-NOTA-daratumumab (range 0.03-100 nM) for 2 h at room temperature. To test the nonspecific binding, 1 μmol of unlabeled daratumumab was added to the corresponding wells. Finally, cells were harvested and counted using an automated

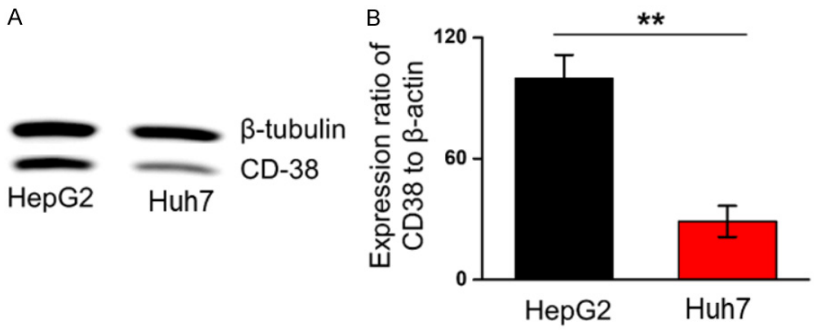

Figure 1. CD38 expression in different liver tumor cells. A. Western blot analysis shows CD38 expression in HepG2 and Huh7 cell line. B. Histogram shows the relative grey-scale value of CD38 bands compared to β-tubulin bands (n=3). **P < 0.01.

γ-counter (PerkinElmer, Waltham, MA, USA). The maximum binding ability (B_{max}), affinity constant (K_a), and receptor density on HepG2 cells were determined using GraphPad Prism software (La Jolla, CA, USA).

Development of the animal tumor model

All animal studies were conducted under the approval of the University of Wisconsin Institutional Animal Care and Use Committee. For tumor implantation, HepG2 and Huh7 cells (1×10^6) were suspended in 100 μL of 1:1 PBS and Matrigel (BD Biosciences), and subcutaneously injected to the lower flank of female athymic nude mice (Envigo, Madison, WI, USA). Tumor size was monitored visually every other day, and in vivo experiments were performed when the tumor reached 5-10 mm in diameter.

PET imaging and image analysis

HepG2 and Huh7 tumor-bearing mice were intravenously injected with 3.7-7.4 MBq of ^{64}Cu-NOTA-daratumumab. PET images were acquired at 6, 12, 24, and 48 h post-injection of ^{64}Cu-NOTA-daratumumab or ^{64}Cu-NOTA-IgG. PET scans of 20-40 million coincidence events were acquired per mouse and PET images were reconstructed using the 3D ordered subset expectation maximization (OSEM3D) algorithm and quantitative region of interest analyses were performed in the Inveon Acquisition Workplace (Siemens Medical Solutions, Malvern, PA, USA).

Ex vivo biodistribution studies

Ex vivo biodistribution studies were performed after the final imaging time point at 48 h post-injection. Mice were euthanized by CO_2 and organs of interest were harvested, including the heart, liver, spleen, kidneys, muscle, and tumor. The portions of these organs were weighed before the activities were counted in an automatic γ-counter, and the results recorded as %ID/g (mean ± SD).

Immunofluorescence staining

In accordance with a previous study, immunofluorescence staining was performed to evaluate CD38 expression [16]. Briefly, tissue slices were fixed, rinsed with PBS, and blocked with 10% donkey serum for 20 min at RT. After being incubated with a primary mouse anti-human anti-CD38 antibody (1:400, Novus Biologicals), these slices were stained with a secondary goat anti-mouse AlexaFluor488 and DAPI, and imaged using a Nikon A1RS confocal microscope.

Statistical analysis

Quantitative data were presented as mean ± standard deviation (SD). Comparisons between tissue uptake data were made using the Student's t-test, where $P < 0.05$ was considered as statistically significant.

Results

CD38 expression in HepG2 and Huh7 cells

Relative expression levels of CD38 in HepG2 and Huh7 cells were evaluated by western blotting. The expression of CD38 in Huh7 cells was only 28.9 ± 7.7% of HepG2 cells, demonstrating the higher expression levels of CD38 in HepG2 compared with Huh7 cells (**Figure 1**).

Binding affinity of daratumumab, NOTA-daratumumab, and ^{64}Cu-NOTA-daratumumab

HepG2 and Huh7 cells were tested by flow cytometry using daratumumab or NOTA-daratumumab as the primary antibody. The high levels of binding affinity were found in HepG2 cells treated with daratumumab or NOTA-daratu-

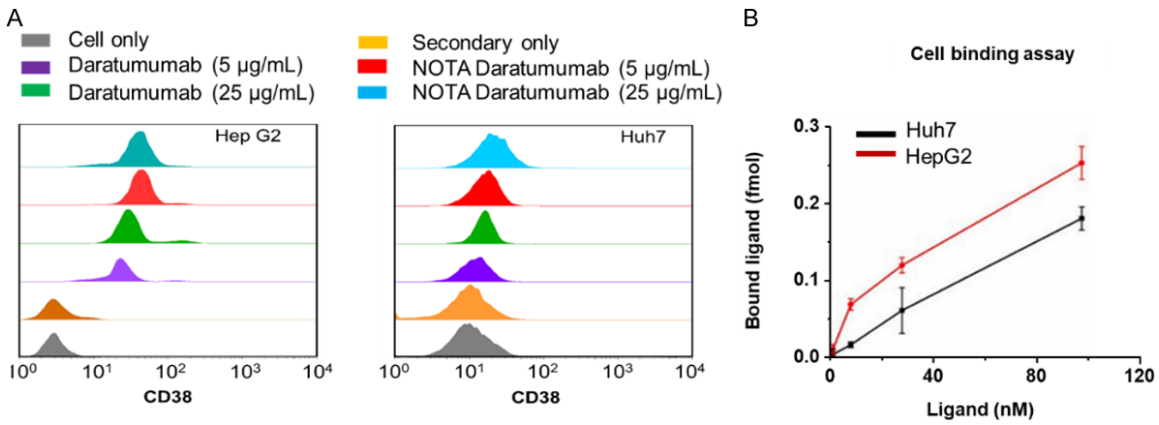

Figure 2. A. Flow cytometry showed differentiated CD38 expression in HepG2 and Huh7 cell lines. Results also verified that NOTA conjugation would not affect CD38 binding of daratumumab. B. Cellular binding assay showed NOTA-conjugated daratumumab bound specifically to HepG2 cells with a K_a value of 18.21 ± 1.74 nM, while the K_a for Huh7 cells was estimated to be 3.98 ± 0.87 μM.

mumab (**Figure 2A**). For HepG2 cells, there is no difference between daratumumab and NOTA-daratumumab. These data suggested that NOTA conjugation had no effect on the binding ability of daratumumab at high or low concentrations.

^{64}Cu-NOTA-daratumumab demonstrated a radiolabeling yield of 89.8 ± 2.2% and the specific activity was in the range of 370-740 MBq/mg (n=11). The receptor binding assay was used for quantifying the B_{max} and K_a of ^{64}Cu-NOTA-daratumumab in HepG2 cells. The specific binding curve revealed that ^{64}Cu-NOTA-daratumumab reached its maximum binding of approximately 0.4 pmol, and the K_a value was 18.21 ± 1.74 nM, with a receptor density of (1.43 ± 0.16) × 10^5 per cell for HepG2 cells (**Figure 2B**), suggesting that ^{64}Cu-NOTA-daratumumab has a high binding affinity for HepG2 cells.

PET imaging of subcutaneous liver tumors

PET imaging was performed at 6, 12, 24, and 48 after injection of ^{64}Cu-NOTA-daratumumab or ^{64}Cu-NOTA-IgG in HepG2 and Huh7 cell line liver tumor models (**Figure 3A**). For HepG2 tumor-bearing mice, ^{64}Cu-NOTA-daratumumab uptakes in tumor were 7.85 ± 0.50, 11.5 ± 1.27, 13.55 ± 1.64, and 13.8 ± 1.49 %ID/g at 6, 12, 24, and 48 h post-injection (n=4), respectively. In mice bearing Huh7 tumors, the average tumor signal was significantly lower at each time point, with 3.50 ± 0.27, 3.98 ± 0.47, 3.95 ± 0.47 and 4.01 ± 0.52 %ID/g at 6, 12, 24, and 48 h post-injection (n=4, $P < 0.01$ when compared with the HepG2), respectively. ^{64}Cu-NOTA-IgG, as non-specific control probe, exhibited a non-specific tumor uptake which was still lower than ^{64}Cu-NOTA-daratumumab in all time points after injection. The passive tumor targeting of IgG antibody was reported previously by our group and was attributed to the enhanced permeability and retention (EPR) effect [17, 21-24]. Non-specific tumor uptake of IgG antibodies depends on the leakiness of vasculature around tumor sites. This means fast growing tumors may have a higher passive uptake of IgG. However, the difference in HepG2 tumor uptakes of daratumumab and non-specific IgG clearly demonstrated a specific accumulation of ^{64}Cu-NOTA-daratumumab for CD38-positive tumor (**Figure 3B**).

Quantitative region-of-interest (ROI) analysis of the blood pool, liver, spleen and kidney was also performed at different time points (**Figure 3C-F**). After injection of ^{64}Cu-NOTA-daratumumab, the uptake in other organs began to decrease, and there were no other significant differences among all three groups.

Biodistribution

To strengthen the PET analysis, ex vivo biodistribution analysis was performed at 48 h post-injection of ^{64}Cu-NOTA-daratumumab (**Figure 4**). The uptake in HepG2 tumors was found to be 13.8 ± 1.5 %ID/g, which was higher than

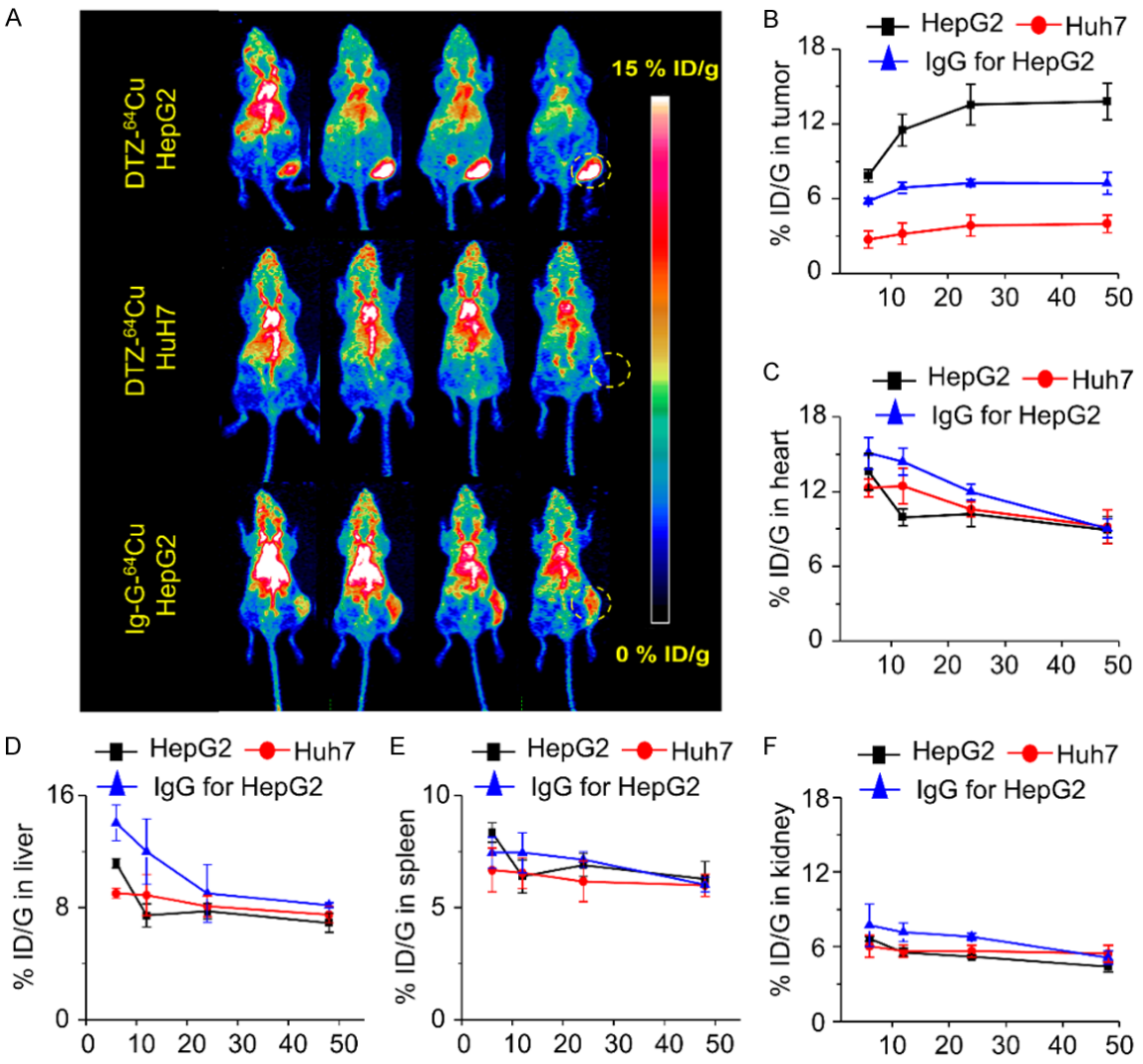

Figure 3. (A) PET maximum intensity projection (MIP) images of HepG2 and Huh7 lymphoma tumor-bearing models from 6 to 48 h post-injection of ^{64}Cu-NOTA-daratumumab (DTZ-^{64}Cu). Quantitative results of PET imaging in tumor (B), heart (C), liver (D), spleen (E) and kidney (F) after injection of ^{64}Cu-NOTA-daratumumab or ^{64}Cu-NOTA-IgG in HepG2 and Huh7 liver tumor models. n=4 per group.

Huh7 tumors at 4.1 ± 0.7 %ID/g ($P < 0.05$, n=4). The tumor uptake of ^{64}Cu-NOTA-IgG in HepG2 tumors was only 7.2 ± 0.9 %ID/g, which is also significantly lower than that of ^{64}Cu-NOTA-daratumumab, suggesting the non-specific binding of IgG in HepG2 tumors. In other organs, including the heart, liver, spleen, and kidneys, ^{64}Cu-NOTA-daratumumab showed a similar trend but lower uptake values in mice bearing HepG2 tumors than those bearing Huh7 tumors, which might be related to the enhanced HepG2 tumor uptake and decreased off-target accumulation.

Immunofluorescence staining of CD38 in tumor tissue

To confirm the differential CD38 expression, different tumor tissues were detected by immunofluorescence staining. We found a higher expression of CD38 in HepG2 tumors than Huh7 tumor tissues (**Figure 5**). This data also demonstrated that there is a correlation between CD38 expression and tumor uptakes, and that the ^{64}Cu-NOTA-daratumumab can be used to visualize non-invasively CD38 in HepG2 tumor tissue.

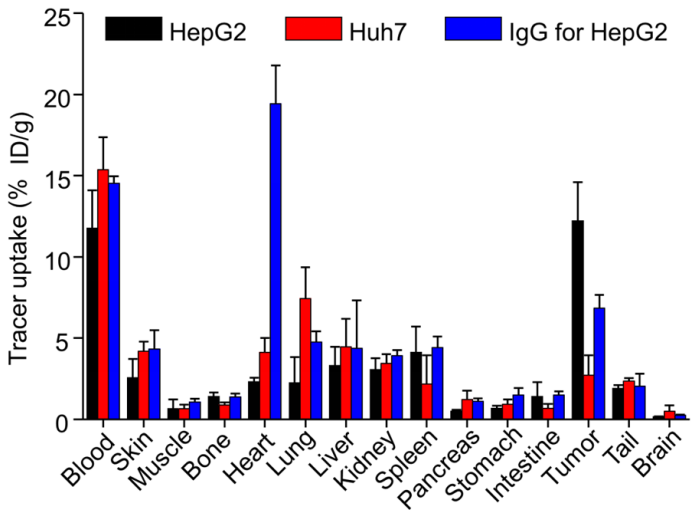

Figure 4. Biodistribution results at 48 h post-injection of ^{64}Cu-NOTA-daratumumab or ^{64}Cu-NOTA-IgG. HepG2 tumors displayed significantly higher uptake than Huh7 tumors and the non-specific IgG group. Relatively high uptake was observed in blood and blood-rich organs, such as heart. **P < 0.01; n=4.

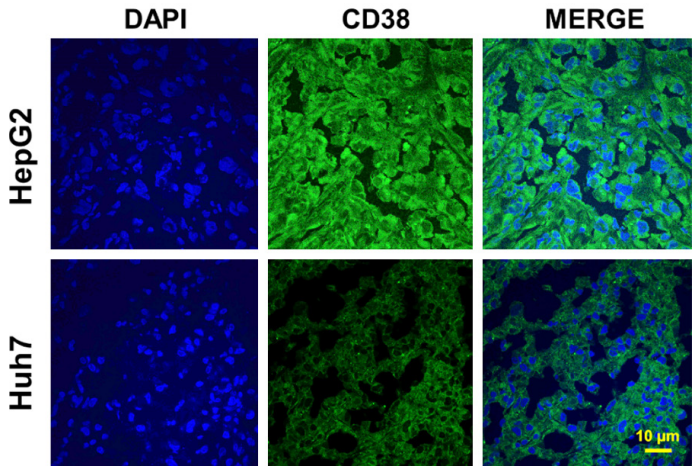

Figure 5. Immunofluorescence staining of tumor tissue sections. HepG2 tumors displayed a high CD38 expression (Green) on the cell surface. Nuclei were stained with DAPI (Blue), Scale bar: 10 μm.

Discussion

Previous research has shown that CD38 is a simple and clinically useful biomarker to diagnose chronic lymphocytic leukemia [25]. However, its association with HCC is still unclear. In this study, we developed a molecular imaging probe to noninvasively detect CD38 expression in HCC in vivo. ^{64}Cu-NOTA-daratumumab was prepared using daratumumab, labeled with a radionuclide (^{64}Cu) and was detected by PET imaging. Importantly, our data demonstrated that ^{64}Cu-NOTA-daratumumab is an effective PET tracer for the non-invasive evaluation of CD38 expression in CD38-positive liver tumor.

Common diagnostic tools, such as X-ray, low-dose whole-body computed tomography (WB-CT) and MRI, are effective ways to detect of myeloma [26, 27], but these methods cannot show molecular changes of the targets. The immune-phenotypic and polymerase chain reaction (PCR)-based molecular techniques are effective tools for CD38 detection in myeloma [16, 28], but they are invasive. Our study showed the ability of ^{64}Cu-NOTA-daratumumab to help visualize the specific expression of CD38 in HepG2 liver tumor models by PET. This immune-PET imaging probe provided a non-invasive method for detecting the CD38^{+} HCC tumor model.

A previous study had demonstrated that the uptake of PET tracers, such as ^{18}F-FDG [29] or ^{99m}Tc-methoxyisobutylisonitrile [30], was related to the level of CD38 expression in some multiple myeloma (MM) clinical studies. However, the quantitative analysis of CD38 expression is still invasive. Therefore, the development of effective tracking agents for CD38 has been a focus in clinical research. Importantly, clinic results have also shown the great potential of daratumumab for imaging research [31]. In addition, our previous studies demonstrated that ^{89}Zr-labeled daratumumab was safe and well-tolerated method for imaging of CD38 expression in lung cancer murine models [32] or B-cell lymphoma [16]. In order to expand on our previous research, ^{64}Cu-NOTA-daratumumab was used for evaluating CD38^{+} HepG2 liver cells. Our data also demonstrated that the higher uptake of ^{64}Cu-NOTA-daratumumab was found in CD38^{+} HepG2 liver tumor than Huh7 liver tumor, suggesting the potential of clinical application for ^{64}Cu-NOTA-daratumumab.

CD38, as transmembrane protein, is also expressed in many hematopoietic lineages

[33]. In addition, it also widely distributed in different tissues and performs receptor function [34]. In some diseases, there is an increased expression of CD38, such as: rheumatoid arthritis synovial tissues [35], systemic lupus erythematosus [36], and liver transplantation rejection [37]. As an immune checkpoint protein, CD38 plays important roles on tumor cell escape from PD-1/PD-L1 blockade [38]. Therefore, immunoPET imaging of CD38 will provide insight into patient-specific evaluation of CD38 expression non-invasively in various CD38-related diseases. In this study, ^{64}Cu-NOTA-daratumumab provided an excellent method to monitor CD38 expression after CD38-targeted treatment.

CD38 therapies have shown their clinical potential to improve efficacy for patients with cancer [38, 39]. However, only a fraction of patients got long-term benefit, and extensive efforts are ongoing to understand the underlying mechanisms of CD38 expression and their relationship to the long-term benefit of CD38 therapy. The ability to track biomarkers effectively for immunotherapy response prediction or CD38^{+} related diseases identification is a key goal for the clinical use of CD38 targeting vectors for diagnosis and combinational therapies. The excellent efficacy in patients treated with daratumumab enhanced the interest in immunotherapy of CD38 combined with radiation treatment. Here in the study, ^{64}Cu-NOTA-daratumumab could provide a simple method for evaluating the response of anti-CD38 treatment, which might yield potential clinical application in the future.

Acknowledgements

This work was supported, in part, by the University of Wisconsin-Madison and the National Institutes of Health (P30CA014520), National Natural Science Foundation of China (81760417, 81660230, 81871031), and Science and Technology Program of Jiangxi, China (2016ACB21019; 2018ACB20020).

Disclosure of conflict of interest

None.

Address correspondence to: Drs. Dawei Jiang and Weibo Cai, Department of Radiology and Medical Physics, University of Wisconsin-Madison, 1111 Highland Avenue, WI, United States. E-mail: djiang29@wisc.edu (DWJ); Tel: 608-262-1749; E-mail: wcai@uwhealth.org (WBC)

References

[1] Zhu RX, Seto WK, Lai CL and Yuen MF. Epidemiology of hepatocellular carcinoma in the asia-pacific region. Gut Liver 2016; 10: 332-339.

[2] Iida-Ueno A, Enomoto M, Tamori A and Kawada N. Hepatitis B virus infection and alcohol consumption. World J Gastroenterol 2017; 23: 2651-2659.

[3] Chu YJ, Yang HI, Wu HC, Lee MH, Liu J, Wang LY, Lu SN, Jen CL, You SL, Santella RM and Chen CJ. Aflatoxin B1 exposure increases the risk of hepatocellular carcinoma associated with hepatitis C virus infection or alcohol consumption. Eur J Cancer 2018; 94: 37-46.

[4] Balogh J, Victor D 3rd, Asham EH, Burroughs SG, Boktour M, Saharia A, Li X, Ghobrial RM and Monsour HP Jr. Hepatocellular carcinoma: a review. J Hepatocell Carcinoma 2016; 3: 41-53.

[5] Bostan N and Mahmood T. An overview about hepatitis C: a devastating virus. Crit Rev Microbiol 2010; 36: 91-133.

[6] Jewell J and Sheron N. Trends in European liver death rates: implications for alcohol policy. Clin Med (Lond) 2010; 10: 259-263.

[7] Yuan H, Lan Y, Li X, Tang J and Liu F. Large hepatocellular carcinoma with local remnants after transarterial chemoembolization: treatment by sorafenib combined with radiofrequency ablation or sorafenib alone. Am J Cancer Res 2019; 9: 791-799.

[8] Jia CC, Chen YH, Cai XR, Li Y, Zheng XF, Yao ZC, Zhao LY, Qiu DB, Xie SJ, Chen WJ, Liu C, Liu QL, Wu XY, Wang TT and Zhang Q. Efficacy of cytokine-induced killer cell-based immunotherapy for hepatocellular carcinoma. Am J Cancer Res 2019; 9: 1254-1265.

[9] Hoshida Y, Nijman SM, Kobayashi M, Chan JA, Brunet JP, Chiang DY, Villanueva A, Newell P, Ikeda K, Hashimoto M, Watanabe G, Gabdoiriel S, Friedman SL, Kumada H, Llovet JM and Golub TR. Integrative transcriptome analysis reveals common molecular subclasses of human hepatocellular carcinoma. Cancer Res 2009; 69: 7385-7392.

[10] Goossens N, Sun X and Hoshida Y. Molecular classification of hepatocellular carcinoma: potential therapeutic implications. Hepat Oncol 2015; 2: 371-379.

[11] Morandi F, Horenstein AL, Costa F, Giuliani N, Pistoia V and Malavasi F. CD38: a target for immunotherapeutic approaches in multiple myeloma. Front Immunol 2018; 9: 2722.

[12] Quarona V, Zaccarello G, Chillemi A, Brunetti E, Singh VK, Ferrero E, Funaro A, Horenstein AL and Malavasi F. CD38 and CD157: a long journey from activation markers to multifunctional molecules. Cytometry B Clin Cytom 2013; 84: 207-217.

[13] Malavasi F, Deaglio S, Funaro A, Ferrero E, Horenstein AL, Ortolan E, Vaisitti T and Aydin S. Evolution and function of the ADP ribosyl cyclase/CD38 gene family in physiology and pathology. Physiol Rev 2008; 88: 841-886.

[14] Shang N, Figini M, Shangguan J, Wang B, Sun C, Pan L, Ma Q and Zhang Z. Dendritic cells based immunotherapy. Am J Cancer Res 2017; 7: 2091-2102.

[15] Malavasi F, Deaglio S, Damle R, Cutrona G, Ferrarini M and Chiorazzi N. CD38 and chronic lymphocytic leukemia: a decade later. Blood 2011; 118: 3470-3478.

[16] Kang L, Jiang D, England CG, Barnhart TE, Yu B, Rosenkrans ZT, Wang R, Engle JW, Xu X, Huang P and Cai W. ImmunoPET imaging of CD38 in murine lymphoma models using (89) Zr-labeled daratumumab. Eur J Nucl Med Mol Imaging 2018; 45: 1372-1381.

[17] England CG, Jiang D, Hernandez R, Sun H, Valdovinos HF, Ehlerding EB, Engle JW, Yang Y, Huang P and Cai W. ImmunoPET imaging of CD146 in murine models of intrapulmonary metastasis of non-small cell lung cancer. Mol Pharm 2017; 14: 3239-3247.

[18] Luo H, Hernandez R, Hong H, Graves SA, Yang Y, England CG, Theuer CP, Nickles RJ and Cai W. Noninvasive brain cancer imaging with a bispecific antibody fragment, generated via click chemistry. Proc Natl Acad Sci U S A 2015; 112: 12806-12811.

[19] Ehlerding EB, Lee HJ, Jiang D, Ferreira CA, Zahm CD, Huang P, Engle JW, McNeel DG and Cai W. Antibody and fragment-based PET imaging of CTLA-4+ T-cells in humanized mouse models. Am J Cancer Res 2019; 9: 53-63.

[20] Zhu H, Zhao C, Liu F, Wang L, Feng J, Zhou Z, Qu L, Shou C and Yang Z. Radiolabeling and evaluation of (64)Cu-DOTA-F56 peptide targeting vascular endothelial growth factor receptor 1 in the molecular imaging of gastric cancer. Am J Cancer Res 2015; 5: 3301-3310.

[21] Jiang D, Im HJ, Sun H, Valdovinos HF, England CG, Ehlerding EB, Nickles RJ, Lee DS, Cho SY, Huang P and Cai W. Radiolabeled pertuzumab for imaging of human epidermal growth factor receptor 2 expression in ovarian cancer. Eur J Nucl Med Mol Imaging 2017; 44: 1296-1305.

[22] Ehlerding EB, England CG, Majewski RL, Valdovinos HF, Jiang D, Liu G, McNeel DG, Nickles RJ and Cai W. ImmunoPET imaging of CTLA-4 expression in mouse models of non-small cell lung cancer. Mol Pharm 2017; 14: 1782-1789.

[23] Kang L, Jiang D, Ehlerding EB, Barnhart TE, Ni D, Engle JW, Wang R, Huang P, Xu X and Cai W. Noninvasive trafficking of brentuximab vedotin and PET imaging of CD30 in lung cancer murine models. Mol Pharm 2018; 15: 1627-1634.

[24] Wei W, Jiang D, Ehlerding EB, Barnhart TE, Yang Y, Engle JW, Luo QY, Huang P and Cai W. CD146-targeted multimodal image-guided photoimmunotherapy of melanoma. Adv Sci (Weinh) 2019; 6: 1801237.

[25] Patten PE, Buggins AG, Richards J, Wotherspoon A, Salisbury J, Mufti GJ, Hamblin TJ and Devereux S. CD38 expression in chronic lymphocytic leukemia is regulated by the tumor microenvironment. Blood 2008; 111: 5173-5181.

[26] Dimopoulos M, Terpos E, Comenzo RL, Tosi P, Beksac M, Sezer O, Siegel D, Lokhorst H, Kumar S, Rajkumar SV, Niesvizky R, Moulopoulos LA, Durie BG; IMWG. International myeloma working group consensus statement and guidelines regarding the current role of imaging techniques in the diagnosis and monitoring of multiple myeloma. Leukemia 2009; 23: 1545-1556.

[27] Dimopoulos MA, Hillengass J, Usmani S, Zamagni E, Lentzsch S, Davies FE, Raje N, Sezer O, Zweegman S, Shah J, Badros A, Shimizu K, Moreau P, Chim CS, Lahuerta JJ, Hou J, Jurczyszyn A, Goldschmidt H, Sonneveld P, Palumbo A, Ludwig H, Cavo M, Barlogie B, Anderson K, Roodman GD, Rajkumar SV, Durie BG and Terpos E. Role of magnetic resonance imaging in the management of patients with multiple myeloma: a consensus statement. J Clin Oncol 2015; 33: 657-664.

[28] Rajkumar SV, Harousseau JL, Durie B, Anderson KC, Dimopoulos M, Kyle R, Blade J, Richardson P, Orlowski R, Siegel D, Jagannath S, Facon T, Avet-Loiseau H, Lonial S, Palumbo A, Zonder J, Ludwig H, Vesole D, Sezer O, Munshi NC, San Miguel J; International Myeloma Workshop Consensus Panel 1. Consensus recommendations for the uniform reporting of clinical trials: report of the International Myeloma Workshop Consensus Panel 1. Blood 2011; 117: 4691-4695.

[29] Ak I and Gulbas Z. F-18 FDG uptake of bone marrow on PET/CT scan: it's correlation with CD38/CD138 expressing myeloma cells in bone marrow of patients with multiple myeloma. Ann Hematol 2011; 90: 81-87.

[30] Ak I, Aslan V, Vardareli E and Gulbas Z. Tc-99m methoxyisobutylisonitrile bone marrow imaging for predicting the levels of myeloma cells in bone marrow in multiple myeloma: correlation with CD38/CD138 expressing myeloma cells. Ann Hematol 2003; 82: 88-92.

[31] Hong H, Severin GW, Yang Y, Engle JW, Zhang Y, Barnhart TE, Liu G, Leigh BR, Nickles RJ and Cai W. Positron emission tomography imaging of CD105 expression with 89Zr-Df-TRC105. Eur J Nucl Med Mol Imaging 2012; 39: 138-148.

[32] Ehlerding EB, England CG, Jiang D, Graves SA, Kang L, Lacognata S, Barnhart TE and Cai W. CD38 as a PET imaging target in lung cancer. Mol Pharm 2017; 14: 2400-2406.

[33] Alessio M, Roggero S, Funaro A, De Monte LB, Peruzzi L, Geuna M and Malavasi F. CD38 molecule: structural and biochemical analysis on human T lymphocytes, thymocytes, and plasma cells. J Immunol 1990; 145: 878-884.

[34] Deaglio S, Mehta K and Malavasi F. Human CD38: a (r)evolutionary story of enzymes and receptors. Leuk Res 2001; 25: 1-12.

[35] Chang X, Yue L, Liu W, Wang Y, Wang L, Xu B, Wang Y, Pan J and Yan X. CD38 and E2F transcription factor 2 have uniquely increased expression in rheumatoid arthritis synovial tissues. Clin Exp Immunol 2014; 176: 222-231.

[36] Pavon EJ, Zumaquero E, Rosal-Vela A, Khoo KM, Cerezo-Wallis D, Garcia-Rodriguez S, Carrascal M, Abian J, Graeff R, Callejas-Rubio JL, Ortego-Centeno N, Malavasi F, Zubiaur M and Sancho J. Increased CD38 expression in T cells and circulating anti-CD38 IgG autoantibodies differentially correlate with distinct cytokine profiles and disease activity in systemic lupus erythematosus patients. Cytokine 2013; 62: 232-243.

[37] Shallis RM, Terry CM and Lim SH. The multifaceted potential of CD38 antibody targeting in multiple myeloma. Cancer Immunol Immunother 2017; 66: 697-703.

[38] Chen L, Diao L, Yang Y, Yi X, Rodriguez BL, Li Y, Villalobos PA, Cascone T, Liu X, Tan L, Lorenzi PL, Huang A, Zhao Q, Peng D, Fradette JJ, Peng DH, Ungewiss C, Roybal J, Tong P, Oba J, Skoulidis F, Peng W, Carter BW, Gay CM, Fan Y, Class CA, Zhu J, Rodriguez-Canales J, Kawakami M, Byers LA, Woodman SE, Papadimitrakopoulou VA, Dmitrovsky E, Wang J, Ullrich SE, Wistuba II, Heymach JV, Qin FX and Gibbons DL. CD38-mediated immunosuppression as a mechanism of tumor cell escape from PD-1/PD-L1 blockade. Cancer Discov 2018; 8: 1156-1175.

[39] Sharma P and Allison JP. The future of immune checkpoint therapy. Science 2015; 348: 56-61.